



The Impact of Surface Loading on GNSS Stations in Africa

SATURDAY E. USIFOH,^{1,2,3} NHUNG LE,^{1,2} BENJAMIN MÄNNEL,¹ PIERRE SAKIC,⁴ JOSEPH DODO,³ and HARALD SCHUH^{1,2}

Abstract—The movement of the Earth’s surface mass, including the atmosphere and oceans, as well as hydrology and glacier melting, causes the redistribution of surface loads, deformation of the solid Earth, and fluctuations in the gravity field. Global Navigation Satellite Systems (GNSS) provide useful information about the movement of the Earth’s surface mass. The impact of surface loading deformation over 145 GNSS sites in Africa was investigated using vertical height time series analysis. The study investigates and quantifies the impact of surface loading on the GNSS coordinates utilizing GNSS Precise Point Positioning (PPP) approach. The German Research Center for Geosciences (GFZ) EPOS.P8 software was used to process and analyze eleven years of GPS data from all the stations, as well as dedicated hydrological and atmospheric loading correction models given by the Earth System Modeling group at Deutsches GeoForschungsZentrum (ESMGFZ). The results of the hydrological loading corrections arising from the surface-deformation were analysed to determine the extent of station improvements. The results revealed about 40% of the stations showed improvement with an average Root Mean Square Error (RMSE) residual of 7.3 mm before the application of the hydrological loading corrections and 7.1 mm Root Mean Square Error (RMSE) after the application of the hydrological loading corrections. Similarly, the atmospheric loading corrections gave an improvement of about 57%. Furthermore, the amplitude values decreased from 4.1–8.1 mm to 3.5–6.2 mm after atmospheric loading corrections. This finding presupposes that applying loading corrections to the derived time series reduces amplitude in some African regions.

Keywords: Surface deformation, GNSS, PPP, time series, hydrological loading, atmospheric loading.

1. Introduction

Seasonal fluctuations in the GNSS time series are caused by uncorrected mass loading deformations, usually comprising atmospheric, hydrological and non-tidal oceanic loading (Fritsche et al., 2012). Another element contributing to seasonal fluctuations in GPS time series is the generation of spurious periodic signals during GPS processing, such as inaccuracies in satellite orbit, tropospheric delay, antenna phase center correction models, and multipath effects. Furthermore, the thermal expansion effect of the bedrock is assumed to be one of the reasons for the periodic shifts in the vertical GPS coordinate time series (Yan et al., 2009). The impacts of different mass loadings vary in different places due to variations in environmental change. The atmospheric, oceanic, and hydrological loadings are key influences in geodynamics investigations (Braitenberg, 2018). Space geodetic techniques have long been utilized to detect surface deformation created by hydrological and atmospheric phenomena (Blewitt, 2003; Dach & Dietrich, 2000). On both short and long periods, hydrological cycles transfer volumes of waters, snow, as well as air all around the world. The gravitational pull on the Earth’s exterior creates elastic deformation of the solid Earth when these masses move. This load-induced surface deformation gives an insight about the Earth and the sources of loading (Blewitt et al., 2001). In the GNSS height time series, surface motions induced through non-tidal atmospheric loading can be detected (Mémin et al., 2020; Tretyak et al., 2021). As a result, loading theory gives a mechanism for comprehending the mass changes between surface water, groundwater, atmosphere, and soil moisture (Braitenberg, 2018; Fritsche et al., 2012; Materna et al., 2021). Regarding the solid Earth, the analysis of the elastic structure of

¹ GFZ German Research Centre for Geosciences, Potsdam, Germany. E-mail: parker@gfz-potsdam.de; satparker@yahoo.com

² Institut für Geodäsie und Geoinformationstechnik, Technische Universität, Berlin, Germany.

³ Centre for Geodesy and Geodynamics, Toro, Bauchi State, Nigeria.

⁴ Institut de Physique du Globe de Paris, Université Paris-Cité, Paris, France.

the crust is made possible by the surface responses to time-varying stresses (Davis et al., 2004). Furthermore, hydrological loading may be a significant source of stress in influencing the time and incidence of earthquakes along with non-volcano tremors (Johnson et al., 2017; Pollitz et al., 2013). Overall, comprehending the hydrological as well as atmospheric loading on geodetic height time series is crucial due to its applications and analysis of lithospheric plate activity.

In the case of crustal tectonic study, deformation caused by surface loading can be isolated against the one generated by an earthquake. The International Earth Rotation and Reference Systems Service (IERS) Convention 2010 (Petit & Luzum, 2010) did not make any recommendation on correcting for non-tidal loading. This could be due to a lack of accessibility of non-tidal models during that period. Surface mass loading causes movements that are not currently taken into consideration for the operational processing of GNSS; hence, loading affects the precision and consistency of the GNSS solution (Blewitt, 2003; Dong et al., 2002; Gruszczynska et al., 2018). In particular, hydrological loading (HYDL) can modify the Earth's surface at millimeter to centimeter scales in two ways. They are elastic and poroelastic loading, which occur when subsurface water influx produces rising refraction in charging the pore spaces while also increasing the fluid tension within the mass beneath, as seen near the aquifer zone (Galloway et al., 1999; Ojha et al., 2019). These methods above all alter the height component of GNSS-based coordinates, with just a modest impact on the horizontal component. One of two approaches utilized in the investigation of hydrological loads is: (1) applying a function to coordinate time series, (such as by estimating the annual and semi-annual amplitudes via sine or cosine functions) or (2) calculating the load via meteorological or hydrological models and estimating the resulting deformation using Green's functions. The second approach, utilizing models given by the German Research Center for Geosciences (ESMGFZ), was used in this study.

Several authors have recently investigated the impact of HYDL corrections over the GNSS coordinates time series in recent years. Jiang et al. (2013) used multiple environmental loading approaches in

assessing surface movements as well as rectifying non-linear fluctuations in the collection of GNSS repeated vertical time series. They discovered that reducing the loading-induced height changes greatly improves the weighted root mean square error (WRMS) values. Notwithstanding, features like river storage, as well as lakes and dam filling, were not accounted for in their models, resulting in amplitudes of a few millimeters being lowered at multiple points along riverbanks. By adjusting at the observation level, Männel et al. (2019) investigated the impact of surface loading on worldwide GNSS as well as VLBI station networks. They obtained a yearly amplitude reduction of roughly 83% of the station time series as well as reduced coordinate repeatabilities of approximately 6 mm for 78% of the time series. Gobron et al. (2021) employed over 10,000 time series to study how aperiodic non-tidal atmospheric loading (NTAL) as well as non-tidal oceanic loading (NTOL) deformations influences the stochastic characteristics on vertical land motion time series. They discovered a 70% reduction in velocity uncertainty in Northern America, Greenland, Fennoscandia, and Antarctica, as well as a significant decrease in the latitude dependency of all stochastic variables. Wu et al. (2020) demonstrated the impact of several loading models on non-linear fluctuations in the GNSS height time series. They discovered that loading corrections possess a positive influence on the decrease of non-linear deformation at a large number of GNSS sites worldwide. Li et al. (2021) studied the impacts of mass loading adjustment on velocity as well as noise parameters. According to the findings, mass loading has a considerable impact on GNSS station velocity.

In Africa, not much work has been done so far on the proportions of surface loading impact on GNSS height time series associated with deformation changes. The purpose of this research is to give a detailed comparison of hydrological and atmospheric loads across Africa using the GNSS coordinate time series. Depending on the region, we investigated this effect and evaluated the efficiency of surface loading to model seasonal deformation at Africa's GNSS stations with partly strong monsoon environments and substantial seasonal deformation. The amplitude of the HYDL and NTAL model was determined and compared with that of GNSS time series. We evaluate

how the model will minimize the GNSS data changes to distinguish vertical from horizontal transients. Following the introduction, Sect. 2 details the area of research, Sect. 3 discusses GNSS and data processing strategies, Sect. 4 discusses results, and Sect. 5 addresses conclusions and recommendations.

2. Area of Research, Data, and Methods

2.1. Area of Research

Africa has a diverse climate due to its location in the northern and southern hemispheres at equatorial and subtropical latitudes. The Holocene climate has been stable in high-latitude zones while the tropics have undergone tremendous hydrological changes in the low-latitude of Africa (Barker et al., 2001). One of the reasons for the changes is the high rainfalls of the African and Indian monsoons which bring moisture to tropical Africa. Additionally, annual raindrop instability correlates to the anomalies in sea surface temperature, pressure, as well as the tropical ocean's zonal circulation (Nicholson, 2000). The monsoon circulations greatly influence climate seasonality as well as its changeability across the African-Indian subcontinent (Fitchett, 2018). They are caused by the force of sea-land intensity gradients at low levels, which is primarily determined by the mean periodic evolution of surface thermal changes. As a result, monsoon systems are frequently represented in a meridional frame where water vapor movement within the Atlantic and Indian oceans causes the Equatorial Convergence Zone to move meridionally, delivering precipitation across the land (Hagos et al., 2014; Martin & Thorncroft, 2014; Webster et al., 1998).

The monsoon, like the rest of Africa's hydrology, has undergone changes over time for several reasons. On a worldwide scale, heating of the Earth near the equator induces tremendous upward motion, as well as convection throughout the monsoon trough or intertropical convergence zone. The northern part of Africa, characterized by aridity and high temperatures, is dominated by warm and hot climates, whereas the northernmost together with the southernmost borders

have a Mediterranean climate. Consequently, by removing the impact of surface loadings (such as hydrological and atmospheric loadings) on the GNSS coordinate time series, we can remove the corresponding annual variations while also reducing common signal noise. Further details will be described in Sect. 4.

2.2. Surface Loading Correction Provided by GFZ

The Earth System Modeling group at Deutsches GeoForschungsZentrum (ESMGFZ), Potsdam, Germany, estimates non-tidal displacements induced by atmospheric, oceanic, together with continental hydrological loading using a patched Green's functions (Farrell, 1972), on a regular basis as described in Dill and Dobslaw (2013). It should be acknowledged that the ESMGFZ displacements field is estimated using the load Love values provided for an elastic Earth model ak135 (Kennett et al., 1995). The surface loading movements are estimated in the center of Earth's figure (CF) reference frame. The estimations are carried out in near-field (0° – 3.5°) on $0.125^{\circ} \times 0.125^{\circ}$ grids, and far-field (3.5° – 180°) using $2.0^{\circ} \times 2.0^{\circ}$ sparse grids. Non-tidal atmospheric loads (NTAL) are calculated using a 3-hourly ECMWF (European Centre for Medium-Range Weather Forecasts) reanalysis of atmospheric surface pressure. The Max-Planck Institute for Meteorology Ocean Model MPIOM (Jungclaus et al., 2013) provides 3-hourly ocean bottom pressure on a global 1.0° grid, which is used to calculate non-tidal oceanic loads (NTOL). Oceanic tides caused by time-varying atmospheric surface pressure were treated in the same way as NTAL. Hydrological loads (HYDL) are based on simulated 24-h terrestrial water storage on a global regular 0.5° grid using the Land Surface Discharged Model (Dill, 2008). Moisture, snow, surface water, and water in lakes and rivers all contribute to mass loads.

Surface deformations in the north, east, and up directions are given with a spatial resolution of 0.5° , and a temporal sampling of 3 h for the atmosphere and ocean, and 24 h for the continental hydrosphere (Dobslaw et al., 2017). Similarly, the ESMGFZ provides corrections for gravity changes and earth

rotation excitations related to the mass ocean (Dill et al., 2018).

3. Processing of Data

We utilized data sets already processed and published in our previous work (Usifoh et al., 2022). A total number of 145 GNSS stations were utilized, and the data were obtained from the AFREF Archive¹ (African Reference Frame Archive), TrigNet² a South African network of continuously operating system stations, as well as EarthScope³ repository (see Fig. 1). Other African GNSS network stations are operational, but their data are not available due to data restrictions.

We use the GFZ EPOS.P8 software to analyze the GNSS data in PPP mode (Männel et al., 2020). The GNSS phase centers provided in igsR3_2135.atx were used to maintain uniformity. Apriori, GNSS orbit products, satellite clocks, and Earth Rotation Parameters (ERP) from GFZ repro3 were introduced (Männel et al., 2021). We used an ionosphere-free linear combination with a 5 min sampling rate on zero-differenced GNSS observations to estimate daily station coordinates as well as tropospheric delays with 1 h ZTD (zenith total delay) in addition to 24 h troposphere gradients. Unresolved phase ambiguities were estimated rather than resolved. We used models following the IERS 2010 Conventions (Petit & Luzum, 2010). Our coordinates are derived in the IGS3 frame because the orbit products are given in the repro3-specific reference frame (Rebischung, 2021). Table 1, contains more information on the processing methodologies.

Position time series were produced utilizing these daily coordinate solutions. We used the GeodeZYX toolbox to convert cartesian (X, Y, Z) coordinates to geodetic (N, E, U) coordinates (Sakic et al., 2019). Following that, Sari software (Santamaría-Gómez, 2019) is used to model station positions by adding (1)

linear velocity b (2) offsets caused by earthquakes, and hardware changes c (3) seasonal variations amplitude d , e (4) and reference coordinate a as expressed on Eq. 1 below.

$$y = a + bt + \sum_{i=1}^N ciGi(t) + d \sin(2\pi t) + e \cos(2\pi t) \quad (1)$$

About 10% of the stations, especially those with repeated offsets, were excluded.

After detrending, we obtained the RMSE average in the north, east and up direction are given in the Table 2 below (Usifoh et al., 2022).

We then compared the derived coordinate time series indicated as GNSS in conjunction with the loading corrected time series (GNSS-HYDL) to evaluate the impact of HYDL. As a measure, the RMSE reduction rate is presented as:

$$RMSE_{reduction} = \frac{RMSE_{GNSS} - RMSE_{GNSS-HYDL}}{RMSE_{GNSS}} \quad (2)$$

Similarly, after the hydrological loadings were removed from the GNSS coordinate time series, the annual amplitude of the GNSS vertical time series changed along with the RMSE reduction rate. The annual amplitude is estimated as:

$$AMP_{reduction} = \frac{AMP_{GNSS} - AMP_{GNSS-HYDL}}{AMP_{GNSS}} \quad (3)$$

The RMSE reduction implies how well the loading time series can explain the signal from the loading models. The larger the RMSE reduction values are, the better the loading models' performance is. When dispersion in the GNSS time series increases by the loading model, the RMS reduction is negative.

4. Results and Discussion

4.1. Spectral Power Density in the Height Component

We use function approximation approaches that combine sine functions and filtering noise to decompose the non-linear properties of the GNSS height coordinate series and derive the harmonic wave

¹ <http://afrefdata.org>: Accessed on the 12.th September, 2022.

² <ftp://ftp.trignet.co.za>: Accessed on then 13.th November, 2022.

³ <https://gage-data.earthscope.org/archive/gnss/rinex/obs>: Accessed on the 10th May, 2023.

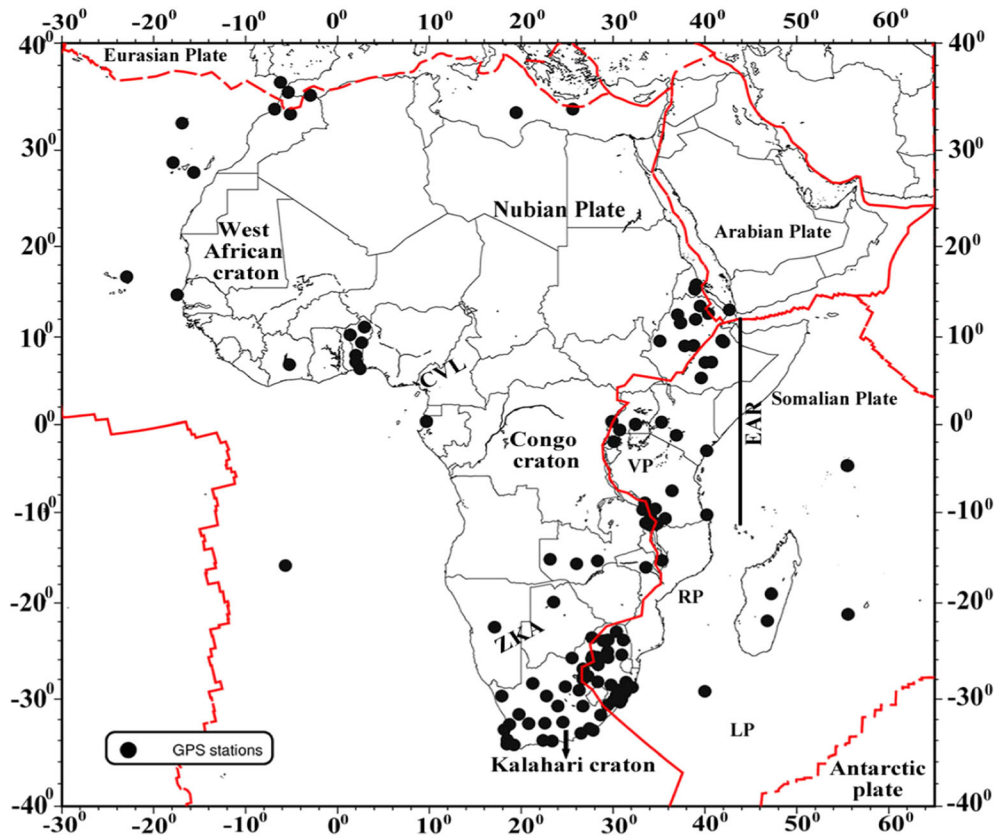


Figure 1
GNSS sites in Africa used in this study

parameters (such as amplitude, phase, and frequency). Figure 2a–f describes the power spectrum density of the GNSS height coordinate series before and after HYDL correction. The wavelet spectrum measures the amplitude of the corrected and non-corrected GNSS height coordinate series. We applied this power spectrum density analysis technique to compare the original GNSS height coordinate series before and after HYDL correction at the three different sites FUNC (Madeira Island, Portugal), SFER (San Fernando, Spain), and MBBC (Mbambe Bay, Tanzania) indicated with red circle in Fig. 1. These stations were selected because (1) we considered their data consistency, and (2) their locations, for example, stations FUNC and SFER are located on an island surrounded by the Atlantic Ocean and salt marshes, and station MBBC is located in one of the microplates, Ruvuma region on the Tanzanian shore of Lake Malawi. To identify the harmonic motion

features of the Earth's crust, we set a spectral frequency in periods of days. For Fig. 2a, b, FUNC, located in Madeira, the North Eastern Atlantic Ocean, 700 km west of the Moroccan coast, we noticed that the magnitude of the annual and semi-annual amplitude before correction is about 1.2 mm and 0.9 mm, respectively, and after corrections, both reduced to about 0.7 mm. This shows that the GNSS height time series appears to be in phase with loading, thus resulting in reduced amplitude. This indicates that GNSS coordinates are not only affected by seasonal signals of terrestrial water storage but also by other loading components, monument stability, and local deformations. But in the high-frequent side of the spectrum, during periods of about 14 days, we noticed a small amplitude of about 1.4 mm. This increment could be due to tidal effects or vibration in the building as this station is placed on the rooftop. In

Table 1
Processing methodologies using GFZ's EPOS.P8

Parameters	Processing strategies
Observations GNSS products GNSS phase center	Ionosphere-free linear combination formed by undifferenced GNSS observation, 5 min sampling, 5° cutoff elevation angle Satellite orbits, clocks, and Earth Rotation parameters (ERP) from GFZ repro3 were introduced a priori Dedicated multi-GNSS ANTEX applied (igsR3_2135.atx)
Ionospheric correction	Ionosphere-free linear combination, second order effect corrected using the International Magnetic Reference Field (11th realization, Finlay et al., 2010)
Tropospheric correction	GPT2 meteo values mapped with VMF1 (Böhm et al., 2006)
Gravity potential	GOCO6s (Kvas et al., 2021)
Solid Earth tides	IERS 2010 Conventions (Petit & Luzum, 2010)
Permanent tide	Conventional tide free
Ocean tide model	FES2014b (Carrère et al., 2016)
Atmospheric tidal loading	S1 and S2 corrections (Ray & Ponte, 2003)
High-frequency EOP model	Desai-Sibois model (Desai & Sibois, 2016)
Mean pole tide	Linear mean pole as adopted by the IERS in 2018
Station coordinates	Freely estimated
GNSS ambiguities	Float solution
Receiver clock	Pre-eliminated every epoch
Non-tidal loading	CF-frame, ESMGFZ (Dobslaw & Dill, 2018), applied to coordinate time series
Cutoff angle	5 degree

Table 2

Statistics of the RMSE in the north, east, and up components of the GNSS,

Statistics	North (mm)	East (mm)	Up (mm)	Ampl. of GNSS (mm)	Ampl. of HYDL (mm)
Average	2.9	9.9	8.5	2.5	2.1
Median	2.4	7.9	6.5	2.1	1.4
Maximum	5.7	30.8	16.6	15.2	6.3
Minimum	1.2	4.7	2.2	0.2	0.4

general, hydrological loading has an effect on this station.

Figure 2c, d, display the power spectrum density of GNSS height coordinate series for the SFER site (San Fernando, Spain) with and without corrections applied. The amplitude of the GNSS height time series is high with about 5.8–3.1 mm, but after the corrections, the amplitude is reduced by a factor of 3 to 1 mm. This significant improvement is related to the station's location in a region with strong signals in terrestrial water storage. For periods shorter than 300 days, the power spectrum density becomes flat, demonstrating a pure white noise in the higher frequencies. This kind of behavior was also reported by Williams et al. (2004) and Klos et al. (2017). For MBBC located in south-eastern Tanzania, two peaks with magnitudes of 7 were observed between periods of 300 and 400 days, however without a clear annual amplitude. But after the corrections, we observed annual and semi-annual amplitudes of about 1.9 mm and 1.5 mm, respectively, corresponding to magnitude 4.2. This shows that after HYDL corrections we are capable of extracting seasonal signals for a better understanding of other geophysical phenomena. This station is located close to the equator; the temperature and precipitation here are not extreme and vary between 20° to 32° and 600 mm to 1800 mm, respectively. The average length of the dry season is between 5 to 6 months. Similarly, from December to March, the northeast monsoon wind brings scorching weather, while the south-east monsoon wind brings occasional rains from March to September. Looking at the downward side of the spectrum with periods of about 14 days, we noticed a small amplitude of about 1.3 mm, which could be due to tidal effects. For the IGS repro3, Rebischung et al. (2021) noted similar amplitudes at a period of 14 day, which are linked to the tidal bands.

4.2. Vertical Variations Due to Hydrological Loading

As discussed in Sect. 4.1, hydrological loading mainly has an effect in the GNSS vertical displacements (Klos et al., 2021; Männel et al., 2019), hence, we examine GNSS height coordinate series to identify seasonal variations of terrestrial water storage across continental Africa. The derived annual amplitudes provide measurable illustrations for

quantifying change in water storage in various climatic zones. As shown in Fig. 3a, the GNSS height coordinate series shows significant annual signals with a maximum amplitude of ~ 8.1 mm (MBBC, Mbamba Bay, Tanzania). This could probably relate to loading independent local or geodynamical processes. One could observe larger amplitudes in East and North Africa than in West and South Africa. According to statistics, the annual amplitude of all the 140 GNSS stations and that of the HYDL is given in Table 2 above. In comparison, the annual amplitude of the HYDL time series is smaller than that of the GNSS height coordinate series as seen in Fig. 3a, b. Furthermore, we observed that RMSE reduction rates were positive at some stations (59), accounting for approximately 42% of the 140 stations. It shows that HYDL has a positive effect in correcting the non-linear deformation of the GNSS height coordinate series at some sites in Africa.

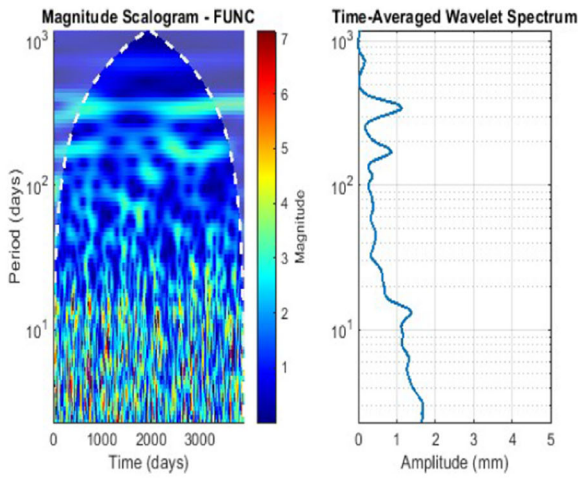
Similarly, we observed that the annual amplitude of the HYDL series (Fig. 3a) was larger in the inland of East as well as West of Africa, namely GNSS stations ABOO, BDAR, and BDMT in Ethiopia (6.3 mm, 5.7 mm, 5.7 mm), ZAMB, Zambia (5.9 mm), TETE, Mozambique (5.9 mm), and BIPA in Republic of Benin (5.8 mm), respectively.

The spatial distribution of GNSS-HYDL for amplitude reduction is displayed in Fig. 3c. The annual amplitude for GNSS-HYDL is 2.2 mm on average. This shows that about 40% of the stations show a reduction compared to the annual amplitude before corrections (2.5 mm). Furthermore, for details analysis, we selected seven stations, MBBC, SFER, SNGC, MZUZ, MELI, IFR1, and SEGY as indicated in Fig. 4, for stations MBBC, SNGC, MZUZ, MELI, and IFR1, we observed largest annual amplitudes of 4.8–8.1 mm, and after applying hydrological loading corrections, their annual amplitudes were reduced to 2.4–3.3 mm. Their percentage reduction rates are indicated in Table 3 below. This means that the HYDL series has an impact on reducing the GNSS annual amplitude. However, the hydrological-driven annual amplitude for station MBBC (Mbamba Bay, Tanzania), located in Western Tanzania, lying on the Eastern bank of Lake Malawi/Lake Nyasa, is about 5.2 mm, while the GNSS coordinates display a substantial deformation of about 8.1 mm. This could

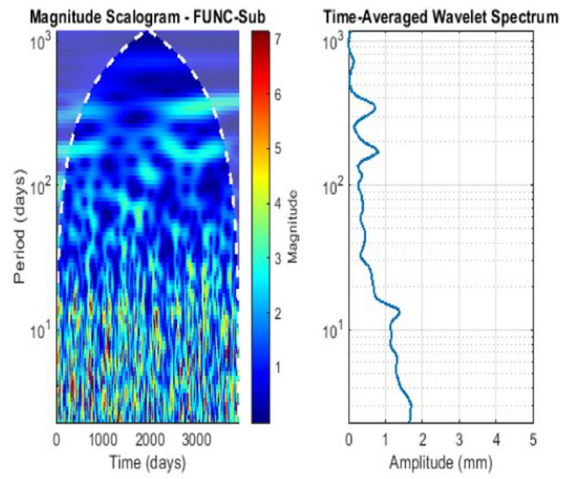
be seen as a result of low-level divergence generated by semi-permanent low-pressure cells centered on Lake Victoria; the station is less impacted by the East African Monsoon region (Awange et al., 2013). Consequently, precipitation is low with westerly winds that bring exceptionally humid air masses from the Congo Basin and a long dry season. For the IGS station MELI (Melilla, Spain), located in North Africa close to the Mediterranean Sea, we observed a very small hydrological-driven deformation of the amplitude of about 2.1 mm, but for PPP coordinates we observed significant amplitudes of about 5.6 mm. The North African Monsoon has an impact on this station, with higher precipitation throughout the boreal summer.

Correcting for the effect of hydrological loading, we observed that amplitudes have a considerable reduction for about 40% of the 140 investigated stations, as these GNSS stations are close to water storages, while almost 60% of the stations have no significant reduction or even exaggerated noise variations like station SEYG. Figure 3c shows the percentage reduction of each station.

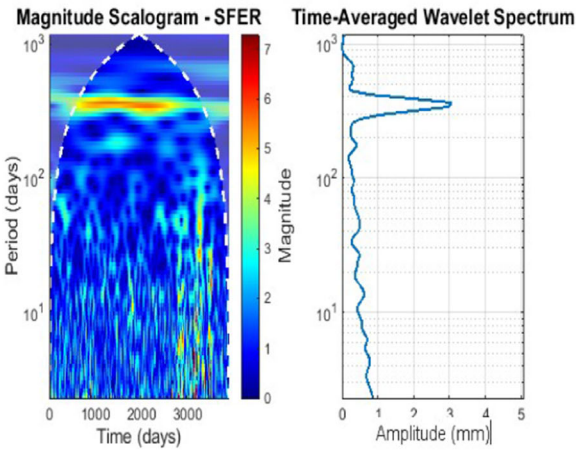
Furthermore, we selected four particular GNSS sites for a comprehensive investigation, by displaying the height coordinates of the station and the modeled deformation produced by terrestrial water storage, see Fig. 5. For stations FUNC (Madeira Island, Portugal) and SFER (San Fernando, Spain) the time series show that their amplitudes are in good agreement for the modeled and the observed height variations. FUNC is almost unaffected by non-tidal loading as explained in Fig. 2a, b with models that provide vertical deformation below 2.2 mm. Similarly, the GNSS coordinate time series is ~ 4.3 mm, and precipitation and rainfall are low. The annual amplitude variations agree with the load-induced deformation quite well (blue curve). Looking at Fig. 5b, SFER (San Fernando, Spain), a station located on the coastline of Mediterranean Sea, Southern Spain, shows consistency between the GNSS station coordinates and the HYDL model. The annual signal in the continental water storage is about 2.6 mm. Based on GNSS, we observe a high annual deformation pattern with an amplitude of 5.8 mm as earlier indicated in Fig. 2c, d. Overall, the coordinates follow almost immediately the loading signal.



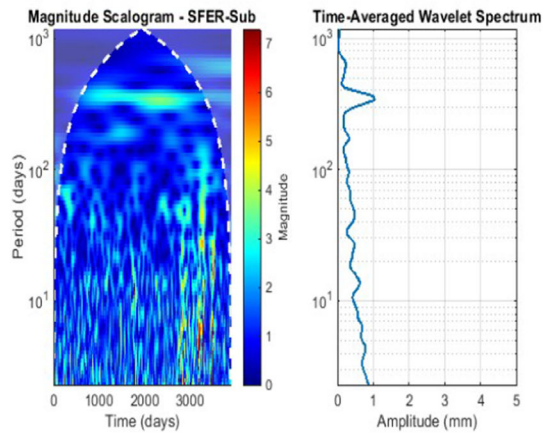
(a)



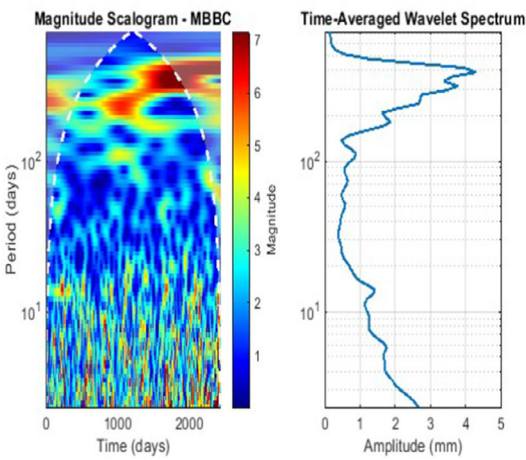
(b)



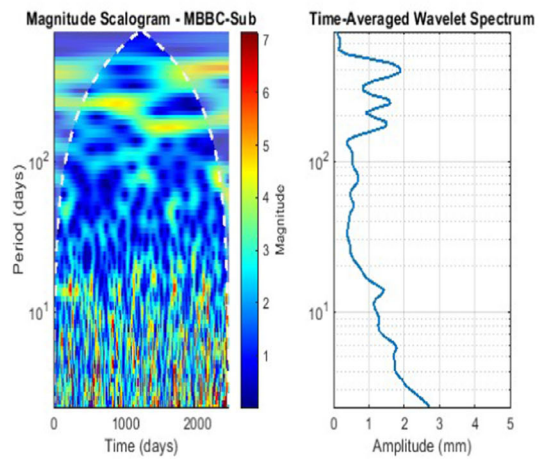
(c)



(d)



(e)



(d)

◀Figure 2

The power spectral density of the GNSS height coordinate series of the selected stations *before* (a,c,e) and *after* (b,d,f) hydrological correction

Also, looking at Fig. 5c, LSMH (Ladysmith, South Africa) is located at KwaZulu-Natal, in the eastern seaboard of South Africa, lapped by the water

of the Indian Ocean seacoast. This station is almost unaffected by HYDL and the model provides vertical deformation of less than 2 mm. Also, the coordinates exhibit considerable deformations up to 2.5 mm, which are likely attributable to loading independent local or geodynamical activities. Here, the sea temperature is relatively stable, with temperatures ranging from 16° to 25 °C in winter, and in summer between September and April, the temperatures range from 23° to 33 °C. The station is above sea level with

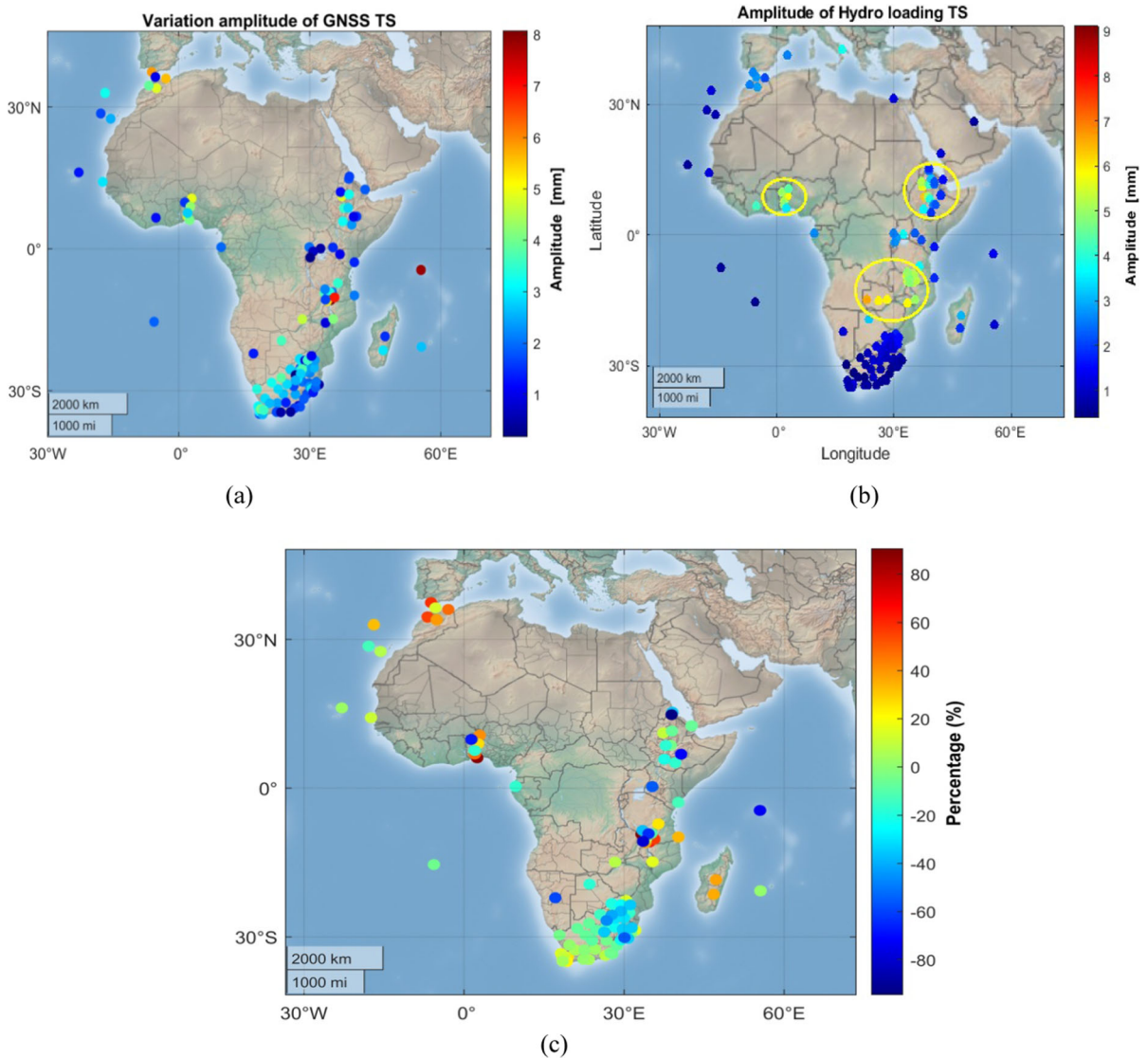


Figure 3

Maps showing annual amplitude of **a** GNSS height time series, **b** HYDL height time series, and **c** percentage amplitude reduction of GNSS height time series

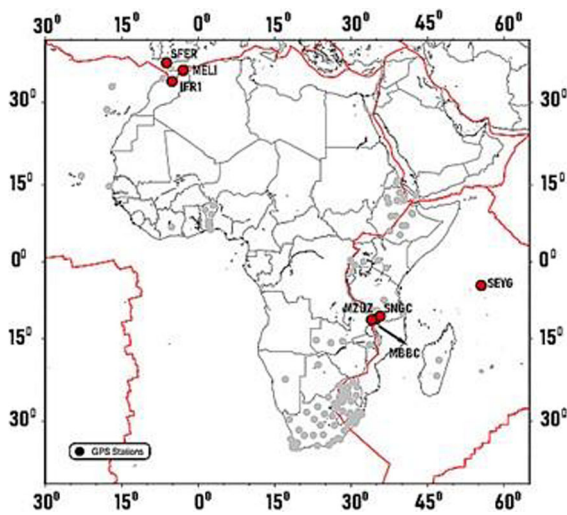


Figure 4

Map of selected stations for amplitude analysis

very low precipitation and rainfall between April and September.

Similarly, for station MBBC (Mbamba Bay, Tanzania), its hydrological-driven deformations reach up to annual amplitude of about 8.1 mm. It has a diverse climate ranging from coastal parts (tropical) to temperate and alpine deserts (on slope of Mount Kilimanjaro), see Table 3 for detailed explanation. Overall, the coordinates follow a periodic pattern, albeit with a peak-to-peak change similar to that of a corrected time series (GNSS-HYDL). This shift may probably be due to local phase inhomogeneities of continental water storage.

For each station, we calculated the RMSE reduction rates using the predicted GNSS coordinates and the HYDL model. The average RMSE residuals

before and after correction are 7.3 mm and 7.1 mm, respectively (Fig. 6a, b). After deducting the hydrological loading correction time series, the stations MARN, South Africa (15.8 mm), MZUZ, Malawi (11.5 mm), and BJNA, BJAB, Republic of Benin (10.7 mm, 10.1 mm), respectively, still have large RMS reduction rates. These could be due to large geophysical anomalies that could cause inaccuracies in deformation modeling.

The impact of HYDL on GNSS height coordinate series in the East as well as North Africa is significant as their RMSE reduction rates are highest, while in the West and South Africa, the hydrological loading corrections have almost no impact (Fig. 6). This could be as a result that Africa is dominated by equatorial low pressure with much annual rainfall and lake waters.

In addition, from the statistics in Fig. 6, the average RMSE reduction values of the East as well as North Africa GNSS stations are 5.4%, and 12.5%, respectively, while in West and South Africa, they are 2.6% and 15.6%, respectively. In general, depending on the region, HYDL has an impact on GNSS height time series.

4.3. Impact of Atmospheric Loading Corrections on Annual Signals

The annual amplitude of all 140 stations coordinate time series is 4.2% on average (Sect. 4.2). The annual amplitude of the NTAL time series is less than that of the GNSS height time series as seen in Fig. 7a, b. The annual amplitude of the NTAL time series for 140 stations is 3.8% on average. Overall, the

Table 3

The annual amplitudes statistics for selected GNSS sites

Sites	(°N)	(°E)	Country	GNSS (mm)	HYDL (mm)	GNSS-HYDL (mm)	Percentage reduction (%)
MBBC	− 11.3	34.8	Tanzania	8.1	5.2	3.0	62.6
SFER	36.5	− 6.2	Spain	5.9	2.7	2.4	58.6
SNGC	− 10.7	35.7	Tanzania	6.9	5.3	2.9	56.9
MZUZ	− 11.4	34.0	Malawi	5.3	4.9	3.3	37.5
MELI	35.3	− 2.9	Spain	5.6	2.1	2.9	47.8
IFR1	33.5	− 5.1	Morocco	4.8	2.8	2.9	38.9
SEYG	− 4.7	55.5	Seychelles	7.9	1.4	13.6	− 74.2

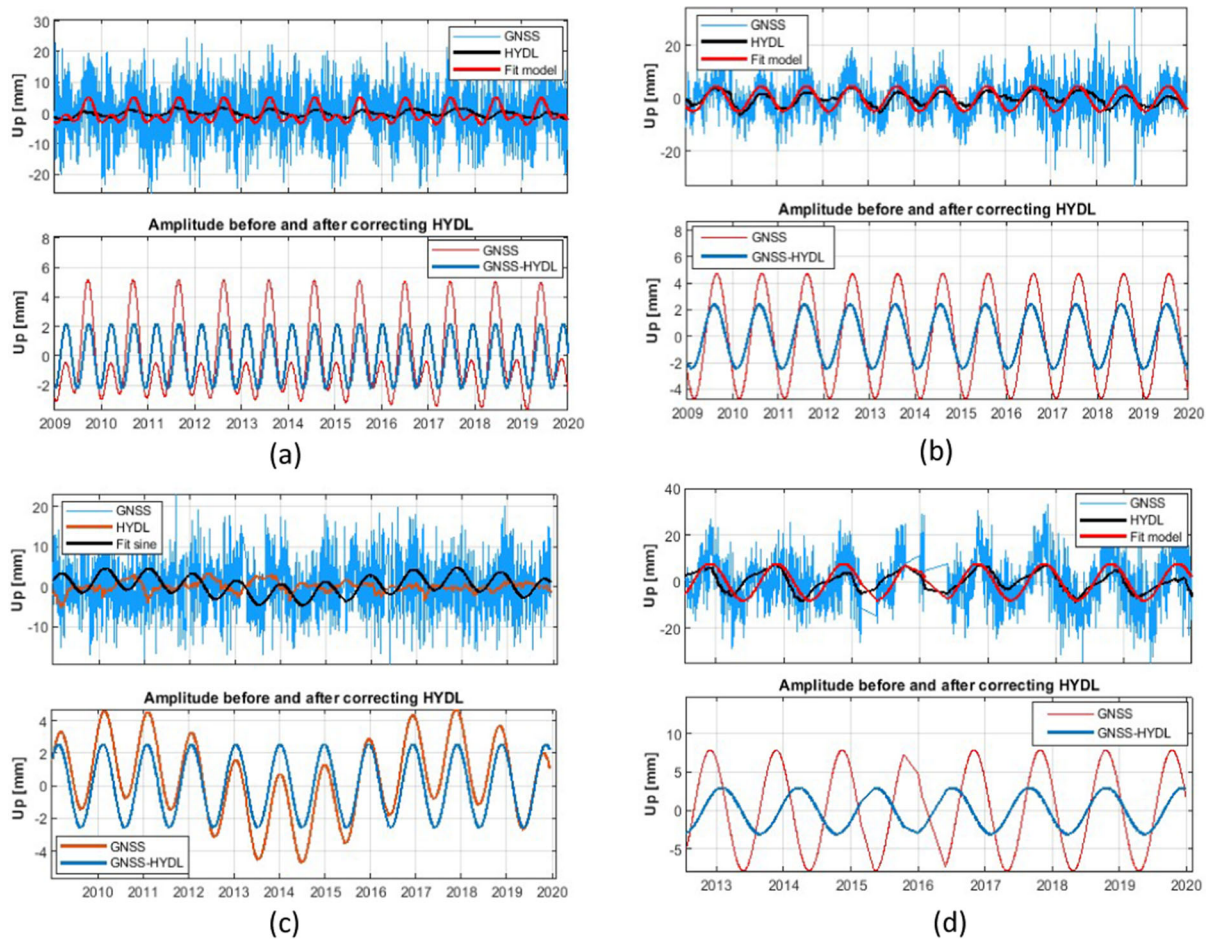


Figure 5

Comparison of station height coordinates. Smooth estimation of heights from PPP GNSS measurement are compared with the computed hydrological model

atmospheric loading could explain about 57% reduction of the GNSS annual amplitude. Before removing the NTAL deformations, see Fig. 7a, the estimated annual amplitudes reach a maximum of about 8.1 mm at station MBBC (Tanzania), and are mostly larger than 1 mm in other stations around the region, while in South Africa and Ethiopia, the estimated annual amplitudes reach about 4 mm.

Figure 7b shows the map of the atmospheric surface deformation during the 11-year study period. The highest changes in atmospheric pressure occur at latitudes 15° with predominantly long-wavelength (Herring et al., 2016). Annual changes in atmospheric pressure are comparatively high at stations ASMA, ASAB, SHEB (Eritrea), and DABT, DAKE

(Ethiopia), with amplitudes of up to 3.0 mm. However, the elastic deformation of solid Earth in reaction to changes in air surface pressure differs across similar geographical locations and also depends on the distance to the coast (Sun et al., 2006). At the equator, the annual amplitude is close to zero, as it is expected that the seasonal behavior pattern is always larger at higher latitudes. Large-scale variation patterns are also observable in South Africa with annual amplitudes of about 2.0 mm.

After loading corrections, see Fig. 7c, we observed larger amplitudes in two stations, SNGC, (Tanzania) and MZUZ (Malawi), with amplitudes of about 7 mm. This did not imply that NTAL corrections introduced new amplitudes to the series;

however, large amplitude estimated based on the uncorrected time series were likely biased low, as a result of deformation activity. GNSS, on the other hand, may contain additional signals that cannot be measured or corrected by the spatial resolution of the NTAL models. Looking at South Africa and Ethiopia, we noticed that a small amplitude reduction of about 3 mm is visible. This could probably be as a result of spatial changes in the noise levels of the GNSS time series. The amplitude is larger in the Northern Cape of South Africa with about 4 mm vertical crustal movement in inland and the magnitude reduces to about 3 mm as it approaches the Coast.

4.4. Change of GNSS Height Time Series

From the preceding analysis, we can noticed, that the loading deformation has a considerable impact on the height component of GNSS sites in Africa. As a result, we examined the height displacement features of NTAL on GNSS stations. The average of these GNSS station coordinates in the height component is stated in Sect. 4.2. Six stations in different regions in Africa were chosen for an extensive study of NTAL

correction; ADIS (Ethiopia), ASMA (Eritrea), BJNA (Republic of Benin), EBBE (Uganda), NURK (Rwanda), and RABT (Morocco), (see Fig. 8). For stations, ADIS, BJNA, EBBE and NURK we observed little reduction in amplitude after applying NTAL correction, while stations ASMA and RABT show no reduction. The reason could probably be due to the quality of the data sets, or due to the location of the monitoring station which is far from the loading source, and the Earth's surface elasticity. For stations EBBE and RABT, their coordinates and velocities show similar linear trends for the corrected and uncorrected time series with changes in their velocities of about 0.04 mm/year. For stations ASMA and BJNA, we observed the same trend with changes in their velocity of about 0.08 and 0.3 mm/year. Moreover, for stations ADIS and NURK, showing subsidence after linear fitting before and after correcting for the time series and their velocities changes are approximately -0.03 mm/year. By investigating the changes in their velocity, we observed that the NTAL causes a small upward trend for ASMA, BJNA, EBBE, and RABT. In contrast, by evaluating the change of their coordinates, we

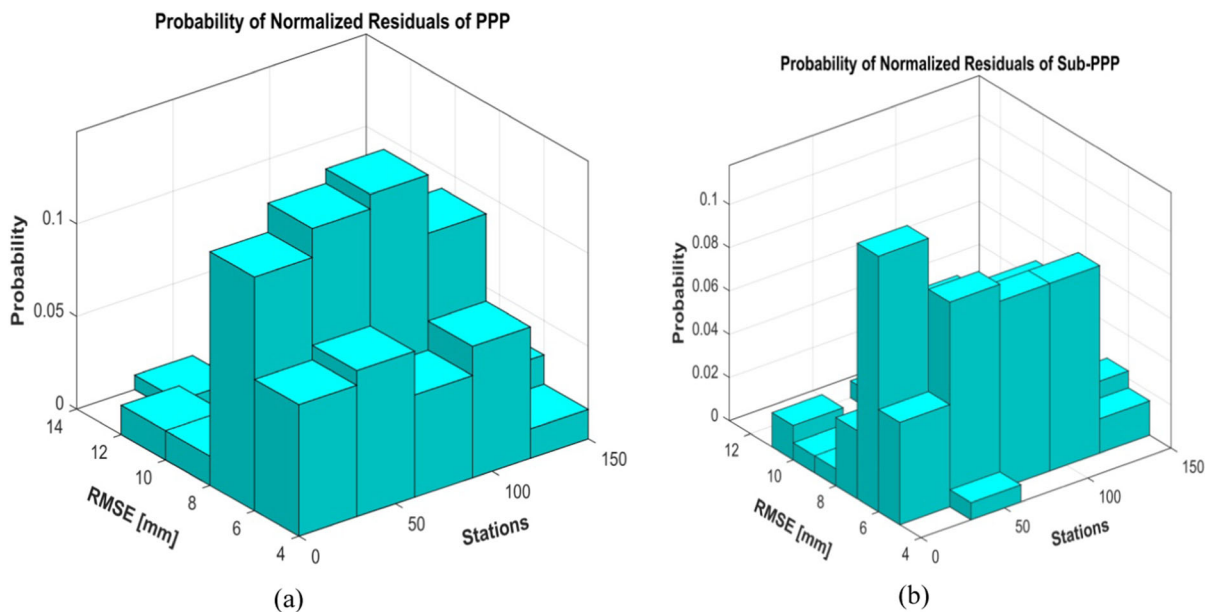


Figure 6

Normalized RMSE residual histograms displaying the percentage reduction rate in East, North, West, and South Africa **a** before and **b** after HYDL corrections

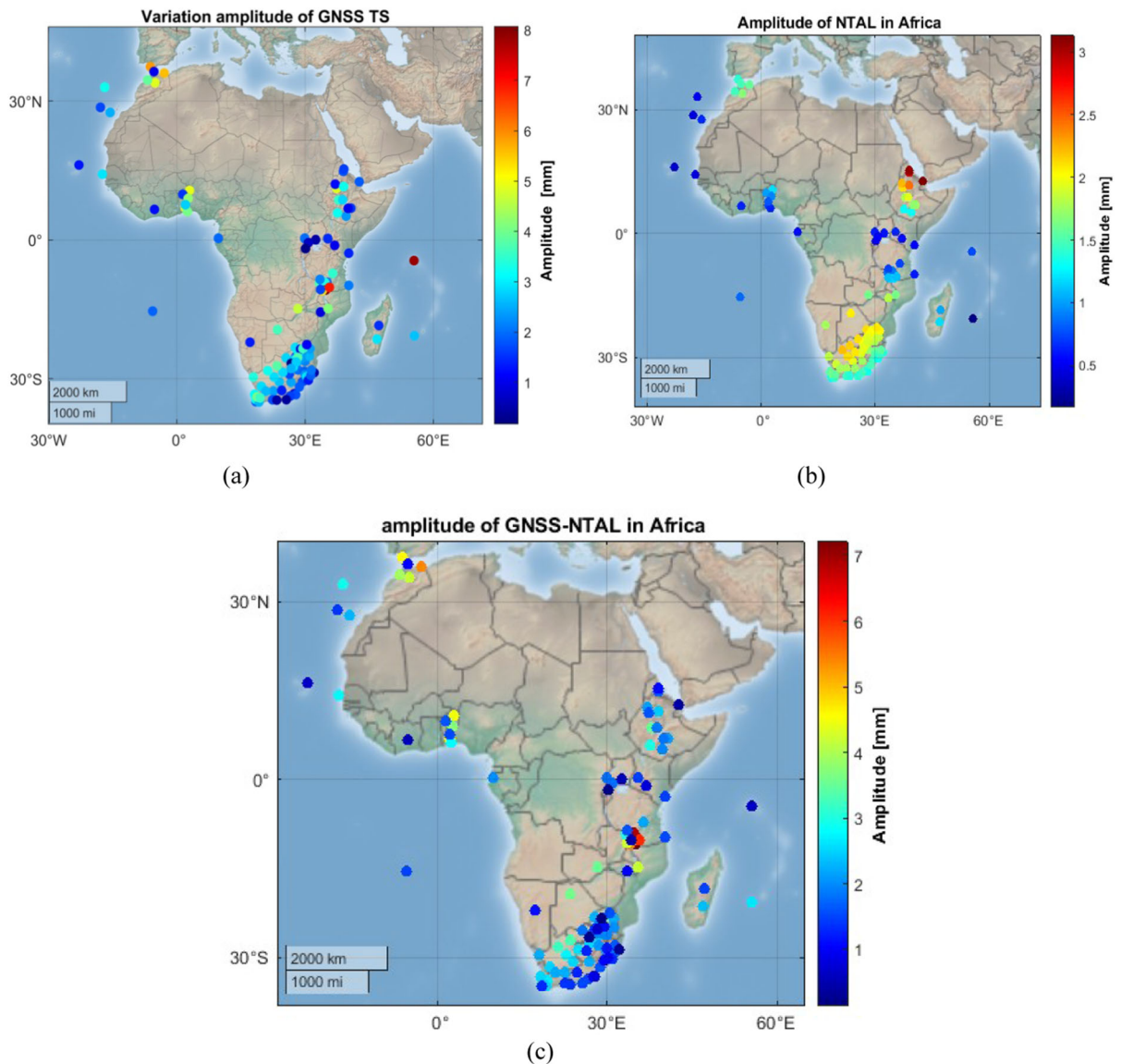


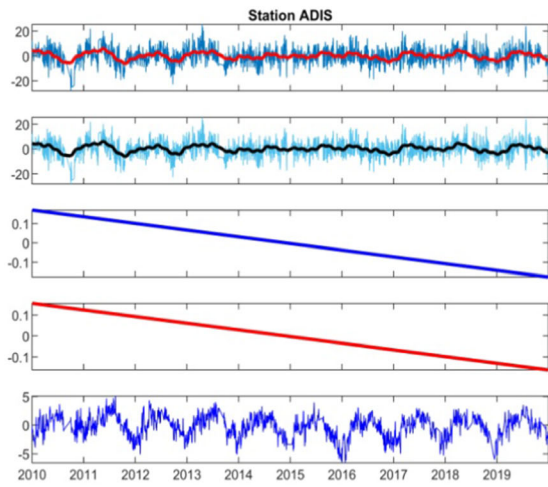
Figure 7

Maps showing annual amplitudes of **a** GNSS height time series, **b** NTAL height time series, and **c** NTAL-corrected GNSS height time series

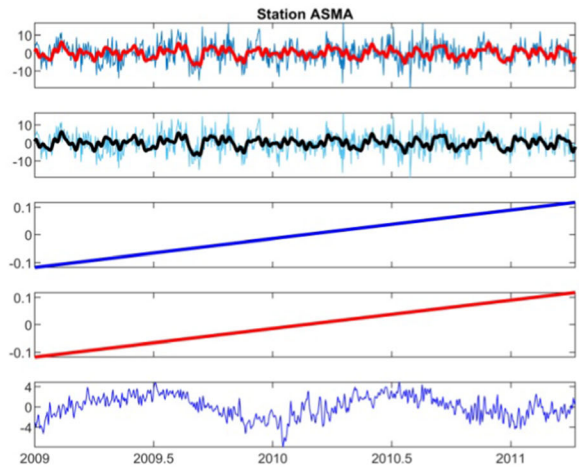
observed that NTAL has little impact on the vertical displacement of these stations.

Station ADIS situated with partially fractured terrain around, exhibits strong vertical displacement when compared to other stations such as BJNA, EBBE, RABT, and ASMA. After loading correction was applied for this station, we observed a downward trend difference of about -0.03 mm/year, and the linear fitting coordinates are mostly the same for the

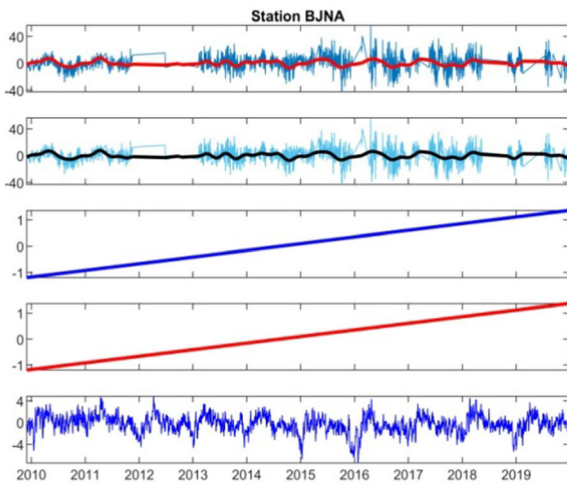
time series with and without correction (plot 2a & 2b, Fig. 8a). The station NURK located in Kigali (Rwanda) exhibits a reversal phenomenon, in which the velocity of the time series after the NTAL correction is less than the original. The reason could be that continental hydrosphere loading is more severe in some places, such as those indicated by the active tectonic setting of the East African Rift.



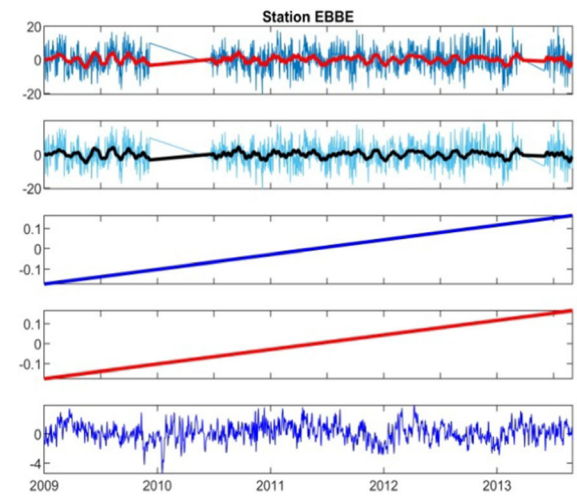
(a)



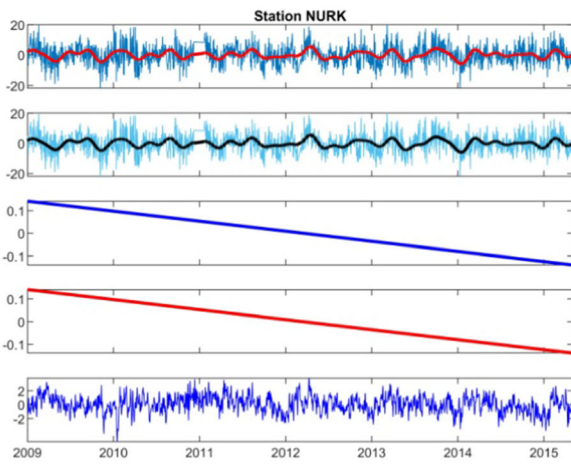
(b)



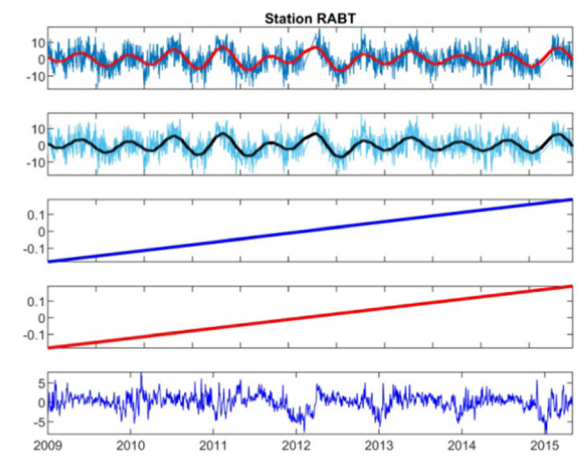
(c)



(d)



(e)



(f)

◀Figure 8

Vertical time series of GNSS stations changes due to NTAL correction. (1) The NTAL (2) linear fitting curve with and without correction, (red and blue lines); (3) residual time series corrected; and (4) up component time series residual uncorrected, red curve was created by fitting a sine function

Table 4 compares the harmonic variation amplitudes and velocities of five GNSS stations across Africa. We apply sine functions to fit the GNSS coordinate time series to identify the motion characteristics of crustal motions with and without correcting the atmospheric loading.

From Table 4, we observed that the change in amplitude for GNSS station IFR1 is substantially smaller compared to other stations, and this may be due to the site location in the Middle Atlas Mountain which consists mostly of a series of limestone plateaus, that is composed of faulted and folded Paleozoic, Mesozoic and Cenozoic rocks. The amplitudes of stations BJAB, IFR1 and MBBC are higher compared to before correction, indicating that the NTAL increases the station's vertical movement to some extent, and changes the values by around 4.1–8.1 mm. For stations SFER and BJKA, an increase in amplitude was demonstrated after correction; this could probably be due to sudden upward crustal movements and changes in watersheds (Caiya et al., 2020).

The vertical motion of stations BJAB, BJKA, IFR1, and SFER are larger than with correction, indicating that the NTAL increases the vertical motion of the station to some degree, and changed the values by around 0.05–0.63 mm/year. For station

MBBC the vertical motion is smaller than before correction, and the change of value by approximately -4.09 mm/year, which was explained in Sect. 4.2.

5. Conclusions

This study examines the peculiar variations of eleven years of GNSS height coordinate series of 140 Africa stations before and after applying hydrological loading corrections, including annual amplitudes and RMSE reduction rate, and allows to drawn conclusions as follow.

Hydrological loading contributes significantly to non-linear changes of the GNSS vertical time series; therefore, applying accurate model of HYDL is vital in improving the GNSS vertical time series. The GNSS-HYDL time series had an average of 2.2 mm amplitudes at 140 stations against 2.5 mm of the original GNSS time series.

The impact of hydrological corrections differs substantially between African GNSS sites. The maximum annual amplitude reduction rate is round 80%, whereas in some stations, non-linear movement rises substantially after applying corrections. For the HYDL as well as the GNSS height coordinate series, a reasonable improvement of around 40% of the GNSS stations was found.

Similarly, using linear regression and GNSS height time series, the impacts of NTAL on crustal motion in Africa were assessed. Based on these, the following characteristics of NTAL on GNSS height time series in various regions were studied:

Based on the investigation, we found that on the average, the amplitude is higher with about 4 mm

Table 4

Fitting parameters for annual with and without corrections of atmospheric loading

Stations	Country	(°N)	(°E)	Amp (mm) uncorrected	Amp (mm) corrected	Vel (mm/year) uncorrected	Vel (mm/year) corrected
BJAB	Rep. of Benin	7.2	2.0	4.6	3.5	- 0.74	- 0.11
B JKA	Rep. of Benin	11.1	2.9	4.5	4.6	- 0.13	0.02
IFR1	Morocco	33.5	- 5.1	4.1	3.5	- 0.03	0.05
MBBC	Tanzania	11.3	34.8	8.1	6.2	4.12	0.01
SFER	Spain	36.5	- 6.2	4.5	4.7	- 0.33	0.18

vertical crustal movement in inland, Northern Cape of South Africa, and the magnitude decreases to approximately 3 mm as it approaches the coast.

The variation in GNSS vertical time series in various zones without and with NTAL correction demonstrated that loading displacement resulted by atmospheric interference had effects on stations BJAB, IFR1 and MBBC, and their amplitudes were considerably reduced after correction. But for stations BJKA and SFER their amplitudes become larger after correction which could be due to sudden vertical crustal movements and changes in watersheds.

That NTAL influence on the linear displacement of the crust on stations ASMA, BJNA, EBBE, and RABT is a small upward trend over time and has little impact on the vertical displacement in these stations. Overall, the atmospheric loading could explain about 57% reduction of the GNSS annual amplitude.

Acknowledgements

The authors wish to express their appreciation to the South African Network (TrigNet), Earthscope, AFREF, and IGS for making their GNSS data available

Author Contributions SU obtained the data, processed it, analyzed it, as well as author the manuscript. The practicality of the approaches was verified by NL, BM, PS, DJ, and HS, together with processing, analysis, interpretation, and discussion of the results. All authors contributed to the manuscript revision and figures alteration.

Funding

Open Access funding enabled and organized by Projekt DEAL. The authors have not disclosed any funding.

Data Availability

<https://afredata.org>: Date access 12th September, 2022. <ftp://ftp.trignent.co.za>: Date access 13th

November, 2022. <https://gage-data.earthscope.org/archive/gnss/rinex/obs>: Date access 10th May, 2023.

Declarations

Conflict of interest There are no conflicts of interest stated by the authors.

Participate consent and ethics approval Not relevant.

Consent to publish Not relevant.

Recognitions The authors wish to express their appreciation to the South African Network (TrigNet), Earthscope, AFREF, and IGS in making their GNSS data available.

Open Access This article is licensed under a Creative Commons Attribution 4.0 International License, which permits use, sharing, adaptation, distribution and reproduction in any medium or format, as long as you give appropriate credit to the original author(s) and the source, provide a link to the Creative Commons licence, and indicate if changes were made. The images or other third party material in this article are included in the article's Creative Commons licence, unless indicated otherwise in a credit line to the material. If material is not included in the article's Creative Commons licence and your intended use is not permitted by statutory regulation or exceeds the permitted use, you will need to obtain permission directly from the copyright holder. To view a copy of this licence, visit <http://creativecommons.org/licenses/by/4.0/>.

Publisher's Note Springer Nature remains neutral with regard to jurisdictional claims in published maps and institutional affiliations.

REFERENCES

- Awange, J. L., Anyal, R., Agola, N., Forootan, E., & Omondi, P. (2013). Potential impacts of climate and environmental change in the stored water of Lake Victoria Basin and economics implication. *Water Resources Research*, 49, 816–8173. <https://doi.org/10.1002/2013WR014350>
- Barker, P. A., Street-Perrott, F. A., Leng, M. J., Greenwood, P. B., Swain, D. L., Perrott, R. A., Telford, R. J., & Ficken, K. J. (2001). A 14,000-year oxygen isotope record from diatom silica in two alpine lakes on Mt. Kenya. *Science*, 292(5526), 2307–2310. <https://doi.org/10.1126/science.1059612>
- Blewitt, G. (2003). Self-consistency in reference frames, geocenter definition, and surface loading of the solid Earth. *JGR Solid Earth*. <https://doi.org/10.1029/2002JB002082>
- Blewitt, G., Lavallée, D., Clarke, P., & Nurudinov, K. (2001). A new global model of Earth deformation: Seasonal cycle detected. *Science*, 294, 2342–2345. <https://doi.org/10.1126/science.1065328>

- Böhm, J., Niell, A. E., Tregoning, P., & Schuh, H. (2006). The global mapping function (GMF): A new empirical mapping function based on data from numerical weather model data. *Geophysical Research Letters*. <https://doi.org/10.1029/2005GL025546>
- Braitenberg, C. (2018). The deforming and rotating earth—a review of the 18th international symposium on geodynamics and earth tide, Trieste 2016. *Geodesy and Geodynamics*. <https://doi.org/10.1016/j.geog.2018.03.003>
- Caiya, Y., Yamin, D., Changhui, X., Shouzhou, G., & Huayang, D. (2020). Effects and correction of Atmospheric pressure loading deformation on GNSS reference stations in Mainland China. *Mathematical Problems in Engineering*, 2020, 4013150. <https://doi.org/10.1155/2020/4013150>
- Carrère, L., Lyard, F., Cancet, M., Guillot, A., Picot, N. (2016). FES2014, a new tidal model—Validation results and perspectives for improvements. In *ESA Living Planet Symposium, Prague, Czech Republic, 9–13 May 2016*
- Dach, R., & Dietrich, R. (2000). Influence of the ocean loading effect on GPS derived precipitable water vapor. *Geophysical Research Letters*, 18, 2953–2958. <https://doi.org/10.1029/1999GL010970>
- Davis, J., Elosegui, P., Mitrovica, J., & Tamisiea, M. (2004). Climate-driven deformation of the solid Earth from GRACE and GPS. *Geophysical Research Letters*. <https://doi.org/10.1029/2004GL021435>
- Desai, S. D., & Sibois, A. E. (2016). Evaluating predicted diurnal and semidiurnal tidal variations in polar motion with GPS-based observations. *Journal of Geophysical Research: Solid Earth*, 121(7), 5237–5256. <https://doi.org/10.1002/2016JB013125>
- Dill, R. (2008). Hydrological model LSDM for operational Earth rotation and gravity field variations. *Scientific Technical Report STR*, vol. 369. GFZ. <https://doi.org/10.2312/GFZ.b103-08095>
- Dill, R., Klemann, V., & Dobsław, H. (2018). Relocation of river storage from global hydrological models to georeferenced river channels for improved load-induced surface displacements. *Journal of Geophysical Research: Solid Earth*, 123(8), 7151–7164. <https://doi.org/10.1029/2018JB016141>
- Dobsław, H., Bergmann-Wolf, I., Dill, R., Poropat, L., Thomas, M., Dahle, C., Esselborn, S., König, R., & Flechtner, F. (2017). A new high-resolution model of non-tidal atmosphere and ocean mass variability for de-aliasing of satellite gravity observations: AODIB RLO6. *Geophysical Journal International*, 211, 263–269. <https://doi.org/10.1093/gji/ggx302>
- Dobsław, H., & Dill, R. (2018). Predicting Earth orientation changes from global forecasts of atmosphere-hydrosphere dynamics. *Advances in Space Research*, 61(4), 1047–1057. <https://doi.org/10.1016/j.asr.2017.11.044>
- Dong, D., Fang, P., Bock, Y., Cheng, M. K., & Miyazaki, S. (2002). Anatomy of apparent seasonal variations from gps-derived site position time series. *Journal of Geophysical Research*, 107(B4), ETG9-1-ETG9-16. <https://doi.org/10.1029/2001JB000573>
- Farrel, W. (1972). Deformation of the Earth by surface loads. *Reviews of Geophysics*, 10(3), 761–797. <https://doi.org/10.1029/RG010i003p00761>
- Finlay, C. C., Maus, S., Beggan, C. D., Bondar, T. N., Chambodut, A., Chernova, T. A., Chulliat, A., Golovkov, V. P., Hamilton, B., Hamoudi, M., Holme, R., Hulot, G., Kuang, W., Langlais, B., & Ilesu, V. (2017). Lühr H, Macmillan S, Manda M, McLean S, Manoj C, Menvielle M, Michaelis I, Oslén N, Rauberg J, Rother M, Sabaka TJ, Tangborn A, Toffner-Clausen L, Thébaud E, Thomson AWP, Wardinski I, Wei Z, Zvereva TI. (2010). International geomagnetic reference field: The eleventh generation. *Geophysical Journal International*, 183, 1216–1230. <https://doi.org/10.1111/j.1365-246X.2010.04804.x>
- Fitchett, J. M. (2018). Recent emergence of CAT5 tropical cyclones in the South Indian Ocean. *South African Journal of Science*, 114(11–12), 1–6. <https://doi.org/10.17159/sajs.2018/4426>
- Fritsche, M., Döll, P., & Dietrich, R. (2012). Global-scale validation of model-based load deformation of the earth's crust from continental water mass and atmospheric pressure variations using GPS. *Journal of Geodynamics*, 59–60, 133–142. <https://doi.org/10.1016/j.jog.2011.04.001>
- Galloway, D., Jones, D. R., Ingebritsen, S. E. (eds) (1999). Land subsidence in the United States. US Geol Surv Circ 1182.
- Gobron, K., Rebischung, P., Van Camp, M., Demoulin, A., & de Viron, O. (2021). Influence of aperiodic non-tidal atmospheric and oceanic loading deformations on the stochastic properties of global GNSS vertical land motion time series. *Journal of Geophysical Research: Solid Earth*, 126, e2021JB22370. <https://doi.org/10.1029/2021JB022370>
- Gruszczynska, M., Rosat, S., Klos, A., Gruszczynski, M., & Bogusz, J. (2018). Multichannel singular spectrum analysis in the estimates of common environmental effect affecting GPS observation. *Geodynamics and Earth Tides Observation from Global to Micro Scale*. <https://doi.org/10.1007/978-3-319-96277-123>
- Hagos, S., Leung, L. R., Xue, Y., Boone, A., de Sales, F., Neupane, N., & Huang, M. (2014). Assessment of uncertainties in the response of the African Monsoon precipitation to land change simulated by a regional model. *Climate Dynamics*, 43, 2765–2775. <https://doi.org/10.1007/s00382-014-2092-x>
- Herring, T. A., Melbourne, T. I., Murray, M. H., Floyd, M. A., Szeli, W. M., King, R. W., Phillips, D. A., Puskas, C. M., Santillan, M., & Wang, L. (2016). Plate Boundary Observatory and related networks: GPS data analysis methods and geodetic products. *Reviews of Geophysics*, 54(4), 759–808. <https://doi.org/10.1002/2016RG000529>
- Jiang, W., Li, Z., van Dam, T., & Ding, W. (2013). Comparative analysis of different environmental loading methods and their impacts on the GPS height time series. *Journal of Geodesy*, 87(7), 687–703. <https://doi.org/10.1007/s00190-013-0642-3>
- Johnson, C. W., Fu, Y., & Bürgmann, R. (2017). Seasonal water storage, stress modulation and California seismicity. *Science*, 356(6343), 1161–1164. <https://doi.org/10.1126/science.aak9547>
- Jungclauss, J. H., Fischer, N., Haak, H., Lohmann, K., Marotzke, J., Matei, D., Mikolajewicz, U., Notz, D., & Storch, J. S. (2013). Characteristics of the ocean simulations in the Max Planck Institute Ocean Model (MPIOM) the ocean component of the MPI-Earth system model. *Journal of Advances in Modeling Earth Systems*, 5(2), 422–446. <https://doi.org/10.1002/jame.20023>
- Kennett, B. L. N., Engdahl, E. R., & Buland, R. (1995). Constraints on seismic velocities in the Earth from travel times. *Geophysical Journal International*, 122(1), 108–124. <https://doi.org/10.1111/j.1365-246X.1995.tb03540.x>
- Klos, A., Gruszczynska, M., Bos, M. S., Boy, J.-P., & Bogusz, J. (2017). Estimates of vertical velocity errors for IGS ITRF2014 stations by applying the improved singular Spectrum Analysis

- method and environmental loading models. *Pure and Applied Geophysics*. <https://doi.org/10.1007/s00024-017-1494-1>
- Klos, A., Karegar, M. A., & Kusche, J. (2021). Quantifying noise in daily GPS height time series: Harmonic function versus GRACE-assimilating modeling approaches. *IEEE Geoscience and Remote Sensing Letters*, *18*, 627–631. <https://doi.org/10.1109/LGRS.2020.2983045>
- Kvas, A., Brockmann, J. M., Krauss, S., Schubert, T., Thomas, G., Meyer, U., Mayer-Gürr, T., Schuh, W.-D., Jäggi, A., & Pail, R. (2021). A satellite-only global gravity field model. *Earth System Science Data*, *13*, 99–118. <https://doi.org/10.5194/essd-13-99-2021>
- Li, Z., Cao, L., & Jiang, S. (2021). Comprehensive analysis of mass loading effects on GPS station coordinate time series using different hydrological loading model. *IEEE Access*. <https://doi.org/10.1109/ACCESS.2021.3067381>
- Männel, B., Brandt, A., Bradke, M., Sakic, P., Brack, A., Nischan, T. (2021). GFZ repro3 product series for the International GNSS Service (IGS. GFZ Data Services). <https://doi.org/10.5880/GFZ.1.1.2021.001>
- Männel, B., Brandt, A., Bradke, M., Sakic, P., Brack, A., & Nischan, T. (2020). Status of IGS reprocessing activities at GFZ. *International Association of Geodesy Symposia*. https://doi.org/10.1007/1345_2020_98
- Männel, B., Dobsław, H., Dill, R., Glaser, S., Balidakis, K., Thomas, M., & Schuh, H. (2019). Correcting surface loading at the observation level: Impact on global GNSS and VLBI station networks. *Journal of Geodesy*, *93*, 2003–2017. <https://doi.org/10.1007/s00190-019-01298-y>
- Martin, E., & Thorncroft, C. (2014). The impact of the AMO on the West African Monsoon annual cycle. *Quarterly Journal of the Royal Meteorological Society*. <https://doi.org/10.1002/qj.2107>
- Materna, K., Feng, L., Lindsley, E. O., Hill, E. M., Ashan, A., Alam, A. K., Oo, K. M., Than, O., Aung, T., Khaing, S. N., & Bürgmann, R. (2021). GNSS characterization of hydrological loading in South and Southeast Asia. *Geophysical Journal International*, *224*(3), 1742–1752. <https://doi.org/10.1093/gji/ggaa500>
- Mémin, A., Boy, J. P., & Santaamaria-Gomez, A. (2020). Correcting GPS measurements for non-tidal loading. *GPS Solution*, *24*, 1–13. <https://doi.org/10.1007/s10291-020-0959-3>
- Nicholson, S. (2000). The nature of rainfall variability over Africa on time scales of decades to millenia. *Global and Planet Change*, *26*(1–3), 137–158. [https://doi.org/10.1016/S0921-8181\(00\)00040-0](https://doi.org/10.1016/S0921-8181(00)00040-0)
- Ojha, C., Werth, S., & Shirzaei, M. (2019). Groundwater loss and aquifer system compaction in San Joaquin Valley During 2012–2015 Drought. *Journal of Geophysical Research*, *124*(3), 3127–3143. <https://doi.org/10.1029/2018JB016083>
- Petit, G., Luzum, B. (2010). IERS Conventions. IERS technical note 36. Verlag des Bundesamts für Kartographie und Geodäsie, Frnakfurt am Main. <https://doi.org/10.1017/S1743921314005535>
- Pollitz, F. F., Wech, A., Kao, H., & Bürgmann, R. (2013). Annual modulation of non-volcanic tremor in northern Cascadia. *Journal of Geophysical Research: Solid Earth*, *118*(5), 2445–2459. <https://doi.org/10.1002/jgrb.50181>
- Ray, R. D., Ponte, R. M. (2003). “Barometric tides from ECMWF operational analysis. In *Annales Geophysicae* (Vol. 21. No. 8, pp. 1897–1910). Göttingen: Copernicus publication. <https://doi.org/10.5194/angeo-21-1897-2003>.
- Rebischung, P. (2021). Terrestrial frame solutions from the IGS third reprocessing. In *EGU General Assembly Conference Abstracts*, pp. EGU21-2144. <https://doi.org/10.5194/egusphere-egu21-2144>
- Rebischung, P., Collilieux, X., Metivier, L., Altamimi, Z., Chanard, K. (2021). Analysis of IGS repro3 Station Position Time Series. Published online Fri. 3 Dec. 2021. <https://doi.org/10.1002/essoar.10509008.1>
- Sakic, P., Ballu, V., Mansur, G. (2019). The GeodeZYX toolbox: A versatile python 3 toolbox for geodetic-oriented purposes. V. 4.0 GFZ Data services. <https://doi.org/10.5880/GFZ.1.1.2019.002>
- Santamaría-Gómez, A. (2019). SARI: interactive GNSS position time series analysis software. *GPS solutions*, *23*(2), 52. <https://doi.org/10.1007/s10291-0846-y>
- Sun, F., Zhu, X., Wang, R., & Li, J. (2006). Detection of changes of the earth’s volume and geometry by using GPS and VLBI data. *Chinese Journal of Geophysics*, *49*, 1015–1021. <https://doi.org/10.1002/cjg2.910>
- Tretyak, K., Brusak, I., Zablotskyi, F. (2021). Impact of non-tidal atmospheric loading on civil engineering structure. <https://doi.org/10.23939/jgd2021.02.016>
- Usifoh, S. E., Männel, B., Sakic, P., Dodo, J., & Schuh, H. (2022). Determination of a GNSS-based velocity field of the african continent. *International Association of Geodesy Symposia*. https://doi.org/10.1007/1345_2022_180
- Webster, P. J., Magaña, V. O., Palmer, T. N., Shukla, J., Tomas, R. M., Yanai, M., & Yasunari, T. (1998). Monsoons: Processes, predictability, and the prospects for prediction. *Journal of Geophysical Research*, *103*(C7), 14451–14510. <https://doi.org/10.1029/97JC02719>
- Williams, S. D. P., Bock, Y., Fang, P., Jamason, P., Nikolaidis, R. M., Prawirodirdjo, L., Miller, M., & Johnson, D. (2004). Error analysis of continuous GPS position time series. *Journal of Geophysical Research*, *109*, B03412. <https://doi.org/10.1029/2003JB002741>
- Wu, S., Guigen, N., Xiaolin, M., Jingnan, L., Yuefan, H., & Changhu, X. (2020). Comparative analysis of the effect of the loading series from GFZ and EOST on long-term gps height time series. *Remote Sensing*, *12*, 2822. <https://doi.org/10.3390/rs12172822>
- Yan, H., Chen, W., Zhu, Y., Zhang, W., & Zhong, M. (2009). Contribution of thermal expansion of monuments and nearby bedrock of observed GPS height changes. *Geophysical Research Letters*, *36*, L13301. <https://doi.org/10.1029/2009GL038152>